Electronic Supplementary Material (ESI) for

Ultrathin Nickel Boron Oxide Nanosheets Vertical Assembled on Graphene: A New Hybrid 2D Materials for Enhanced Photo/electro-catalysis

Min-Quan Yang,[a] Jiadong Dan[b] Stephen J. Pennycook,[b] Xin Lu,[a] Hai Zhu,[c] Qing-Hua Xu,[c] Hong Jin Fan,[d] and Ghim Wei Ho[a]*

[a]*Department of Electrical and Computer Engineering, National University of Singapore, 4 Engineering Drive 3, 117583 Singapore, Singapore*
E-mail: elehgw@nus.edu.sg
[b]*Department of Materials Science and Engineering, National University of Singapore, 9 Engineering Drive 1, 117575 Singapore, Singapore*
[c]*Department of Chemistry, National University of Singapore, 3 Science Drive 3, 117543 Singapore, Singapore*
[d]*School of Physical and Mathematical Sciences, Nanyang Technological University, 21 Nanyang Link, 637371 Singapore, Singapore*

Experimental Section

Materials: Nickel nitrate hexahydrate ($Ni(NO_3)_2\cdot 6H_2O$), sodium borohydride ($NaBH_4$), potassium persulfate ($K_2S_2O_8$), phosphorus pentoxide (P_2O_5), potassium permanganate ($KMnO_4$), hydrogen peroxide (H_2O_2, 30%), nitric acid (HNO_3, 65%), absolute ethanol (C_2H_5OH), triethanolamine (TEOA), and Eosin Y (EY) were all purchased from Sigma-Aldrich Corporation. Sulfuric acid (H_2SO_4) and hydrochloric acid (HCl) were obtained from Fisher Scientific. Potassium hydroxide (KOH) was purchased from ACROS Organics. Graphite powder was supplied from Qingdao Zhongtian Company, China. All chemicals were used as received without further purification. The deionized (DI) water used throughout experiments was from local source.

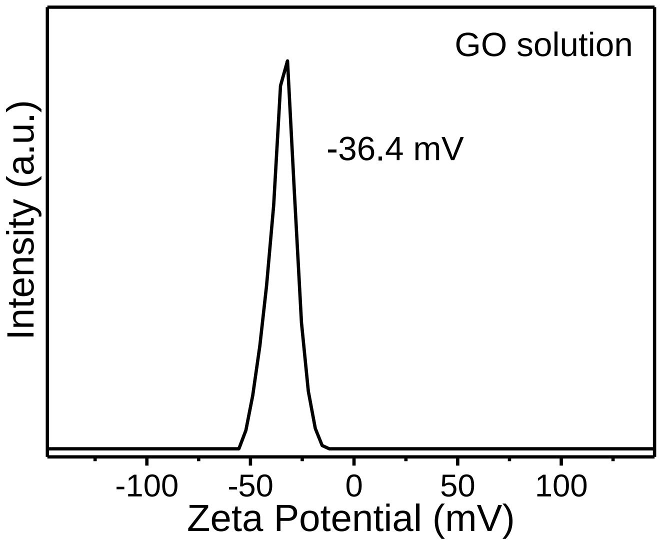

Fig. S1 Zeta potential of graphene oxide (GO) dispersed in deionized water.

The dispersion of GO in water reveals a strong negatively charged surface with a zeta potential value of -36.4 mV, which is stemmed from the large amount of oxygenated functional groups (e.g., epoxy, carboxyl and hydroxyl groups) on the GO surface. The negatively charged surface endows GO to be well dispersed in the aqueous solution and facilitates the adsorption of positively charged Ni^{2+} through strong electrostatic interaction between them.

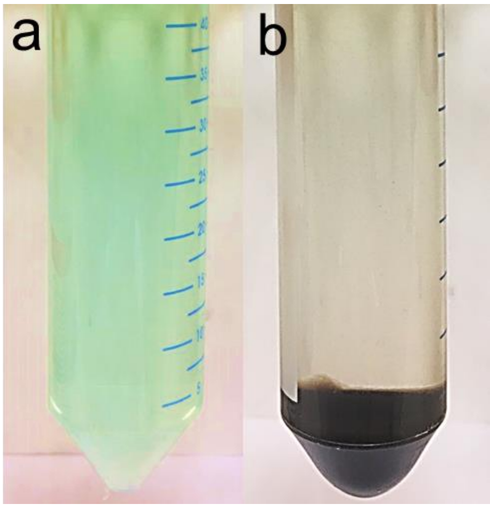

Fig. S2 Digital photograph of nickel nitrate (Ni^{2+}) solution (a) before and (b) after the addition of graphene oxide (GO).

The colorless supernatant of the nickel nitrate solution with the addition of graphene oxide after mixing 3 mins indicates the fast and strong adsorption of Ni^{2+} over GO.

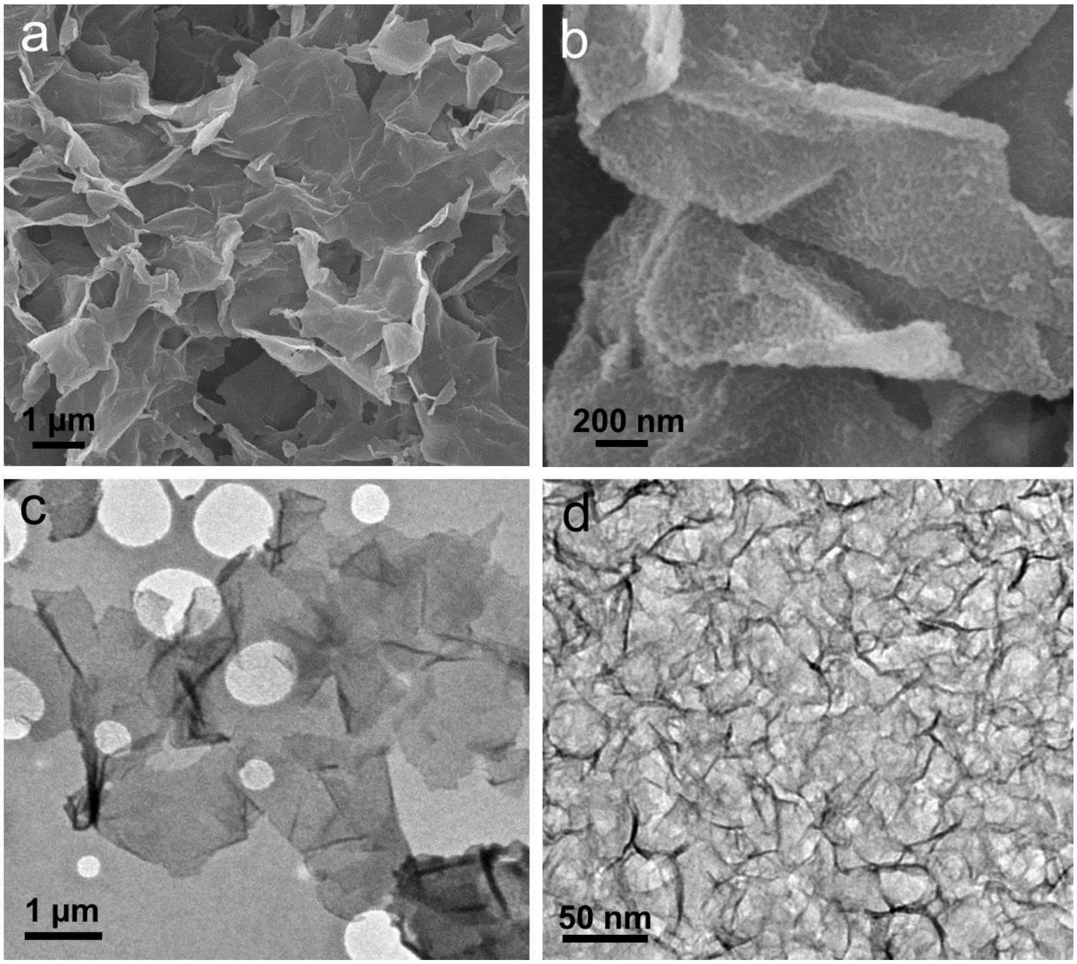

Fig. S3 (a,b) Scanning electron microscopy (SEM) images and (c,d) transmission electron microscopy (TEM) images of Ni-B_i/G in large scale.

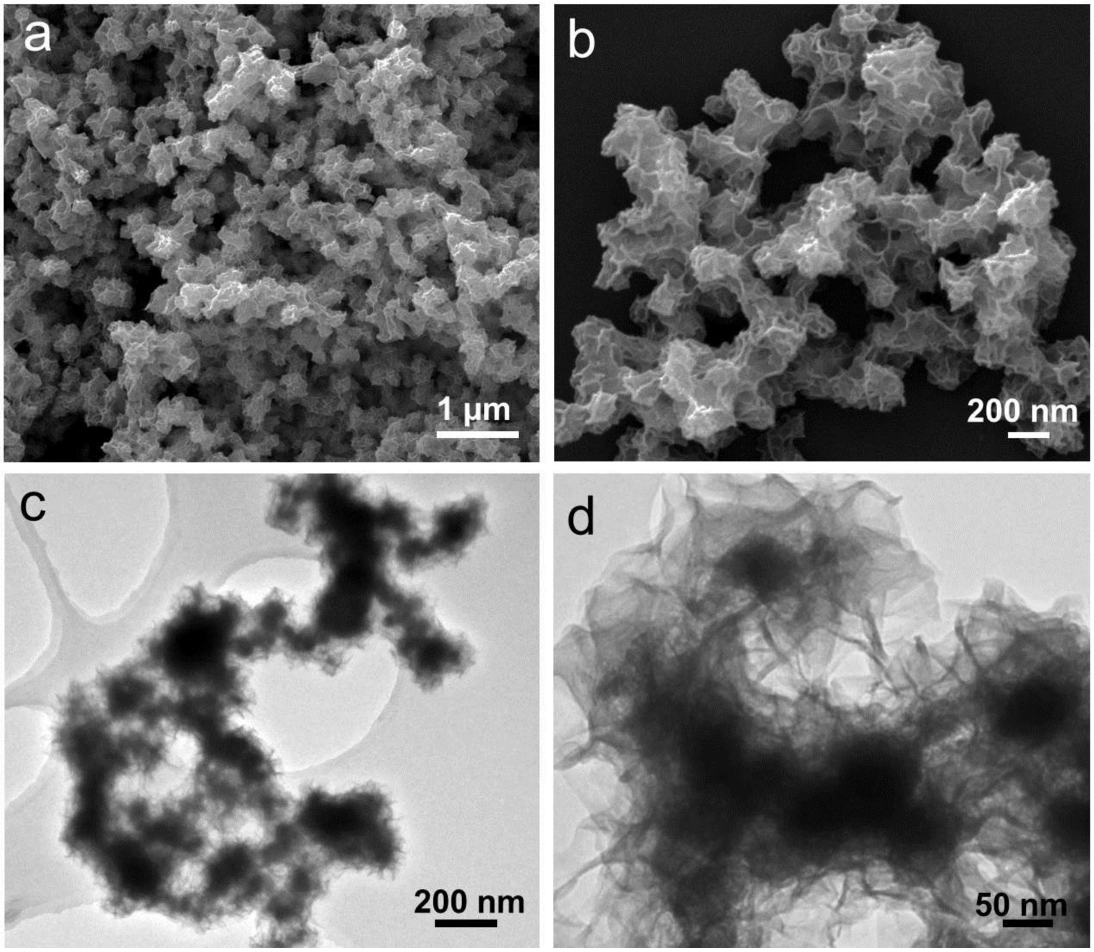

Fig. S4 (a,b) Scanning electron microscopy (SEM) images and (c,d) transmission electron microscopy (TEM) images of Ni-B_i in large scale.

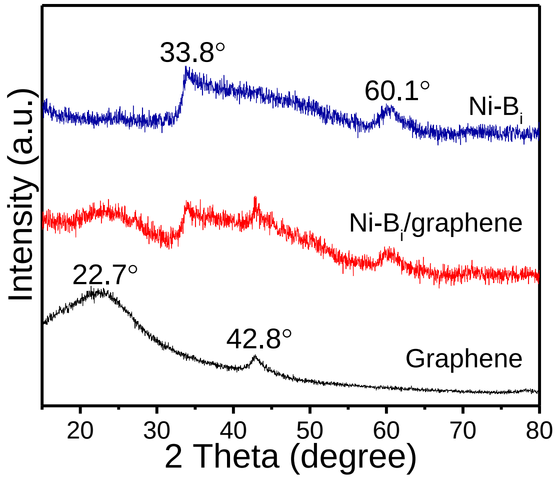

Fig. S5 X-ray diffraction (XRD) patterns of the blank Ni-B$_i$, hybrid Ni-B$_i$/graphene and graphene. The similar broad and weak peaks at 33.8° and 60.1° in both the spectra of blank Ni-B$_i$ and the hybrid Ni-B$_i$/graphene can be indexed to amorphous phase nickel boron oxide and match well with the reported data.[S1] Two additional peaks at 22.7° and 42.8° appearing in the Ni-B$_i$/graphene spectrum corresponds to the typical diffraction peaks of graphene.[S2, S3]

The XRD result demonstrates that the introduction of graphene during the synthesis process has no influence on the crystal nature of the nickel boron oxide, confirming the hybridization of Ni-B$_i$ with graphene forming the 2D Ni-B$_i$/graphene hybrid composite.

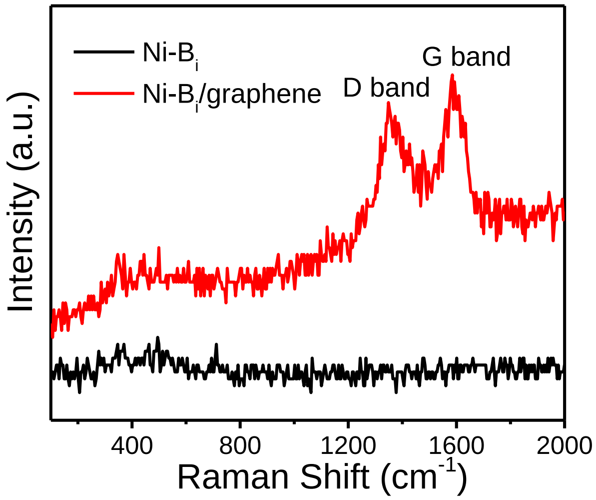

Fig. S6 Raman spectra of the blank Ni-B$_i$ and hybrid Ni-B$_i$/graphene.

No obvious characteristic peaks are observed in the Raman spectrum of blank Ni-B$_i$. Only two characteristic D (1354 cm^{-1}) and G bands (1586 cm^{-1}) of graphene[S4] are detected in the hybrid Ni-B$_i$/graphene sample. Therefore, the nickel boron oxide in both samples are amorphous.

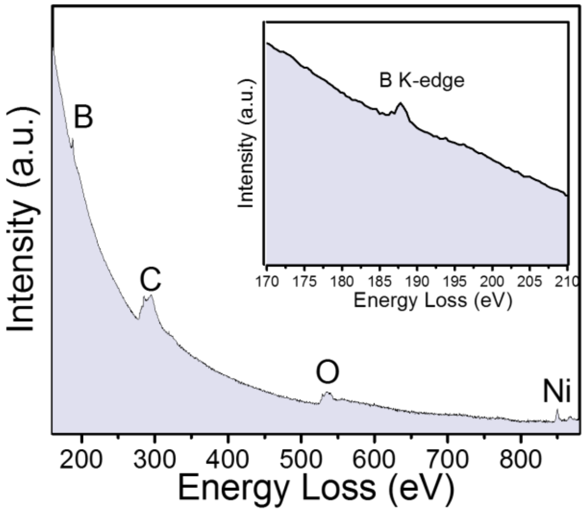

Fig. S7 Electron energy loss spectroscopy (EELS) spectrum of Ni-B$_i$/G heterostructure; inset is the high-resolution spectrum of B K-edge.

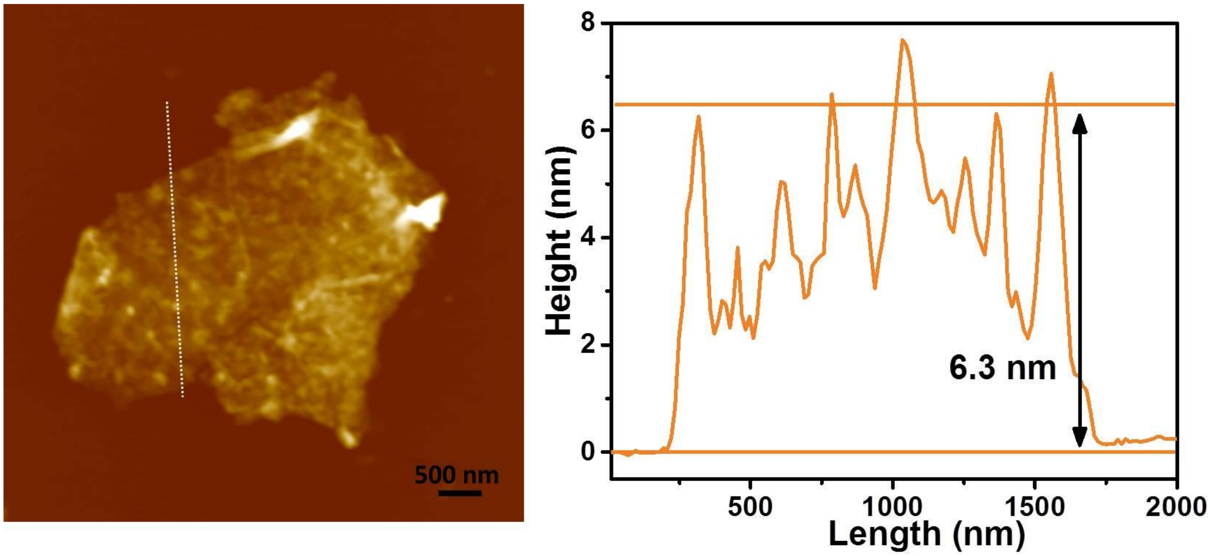

Fig. S8 Atomic force microscopy (AFM) image and height profile of Ni-B_i/30%G heterostructure.

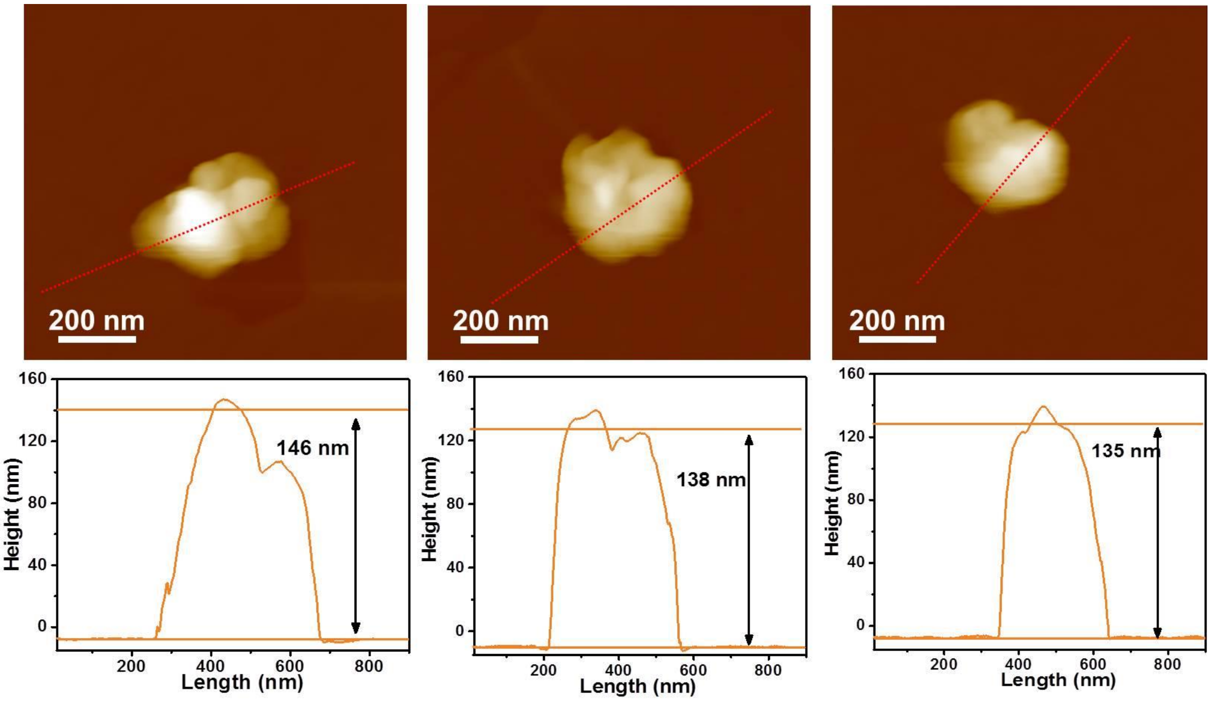

Fig. S9 Atomic force microscopy (AFM) images and height profiles of blank Ni-B_i.

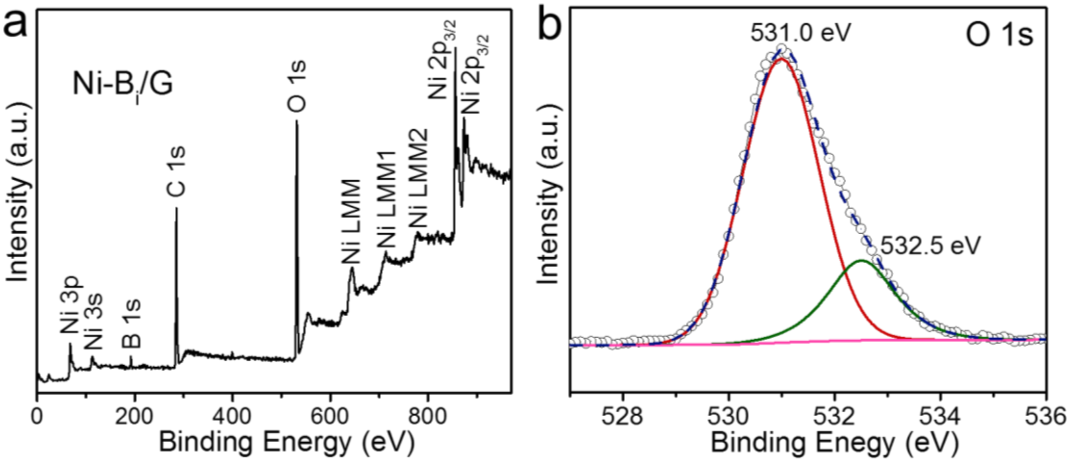

Fig. S10 X-ray photoelectron (XPS) survey (a) and O 1s (b) spectra of the as-prepared Ni-B_i/G heterostructure.

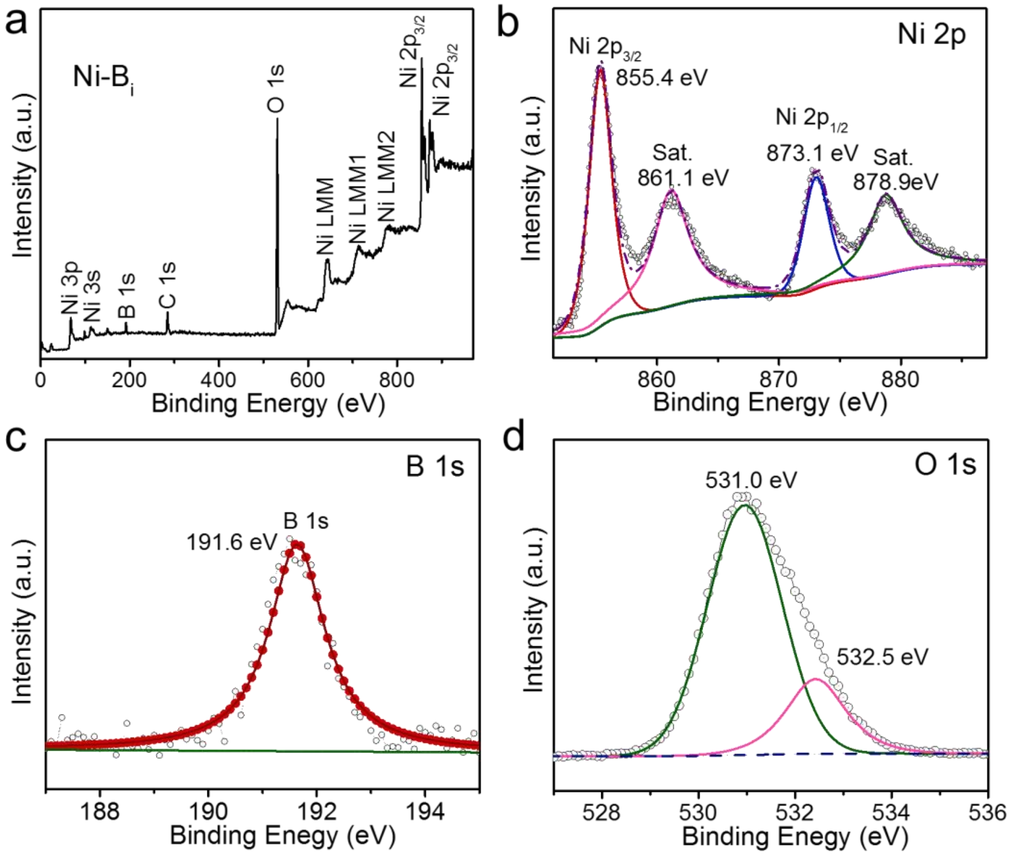

Fig. S11 X-ray photoelectron (XPS) survey (a) spectrum, high-resolution Ni 2p (b), B 1s (c) and O 1s (d) spectra of the as-prepared blank Ni-B_i sample.

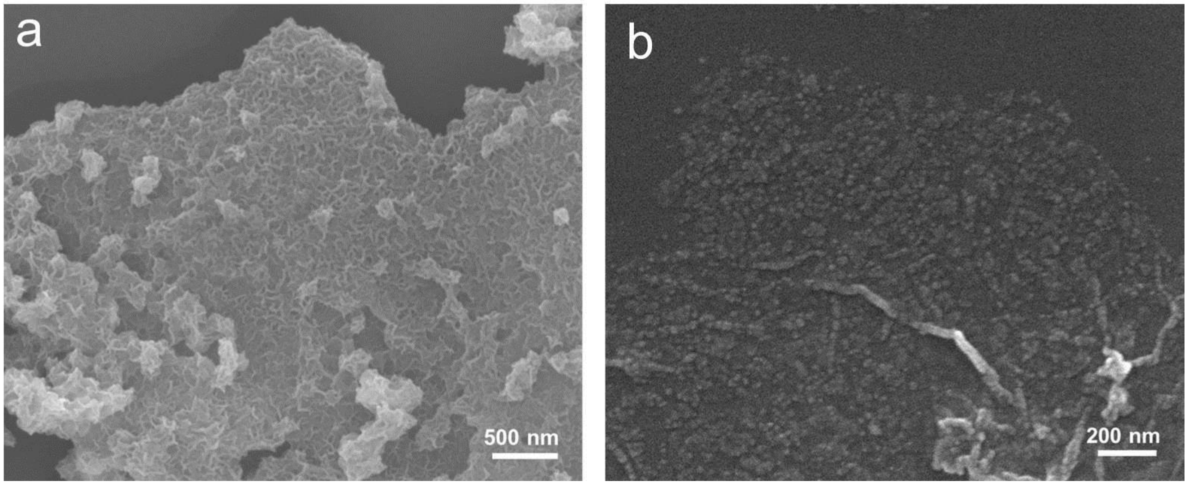

Fig. S12 Scanning electron microscopy (SEM) images of Ni-B$_i$/10%G (a) and Ni-B$_i$/50%G (b).

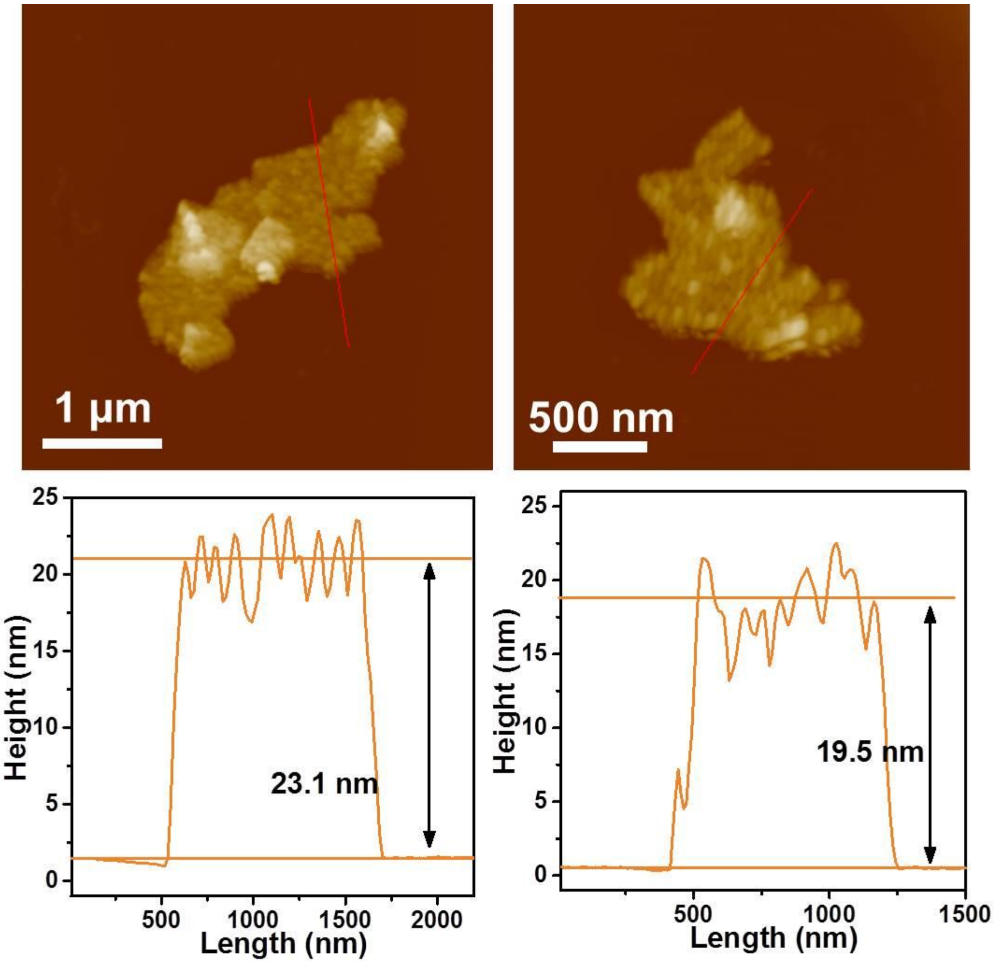

Fig. S13 Atomic force microscopy (AFM) images and height profiles of Ni-B$_i$/10%G.

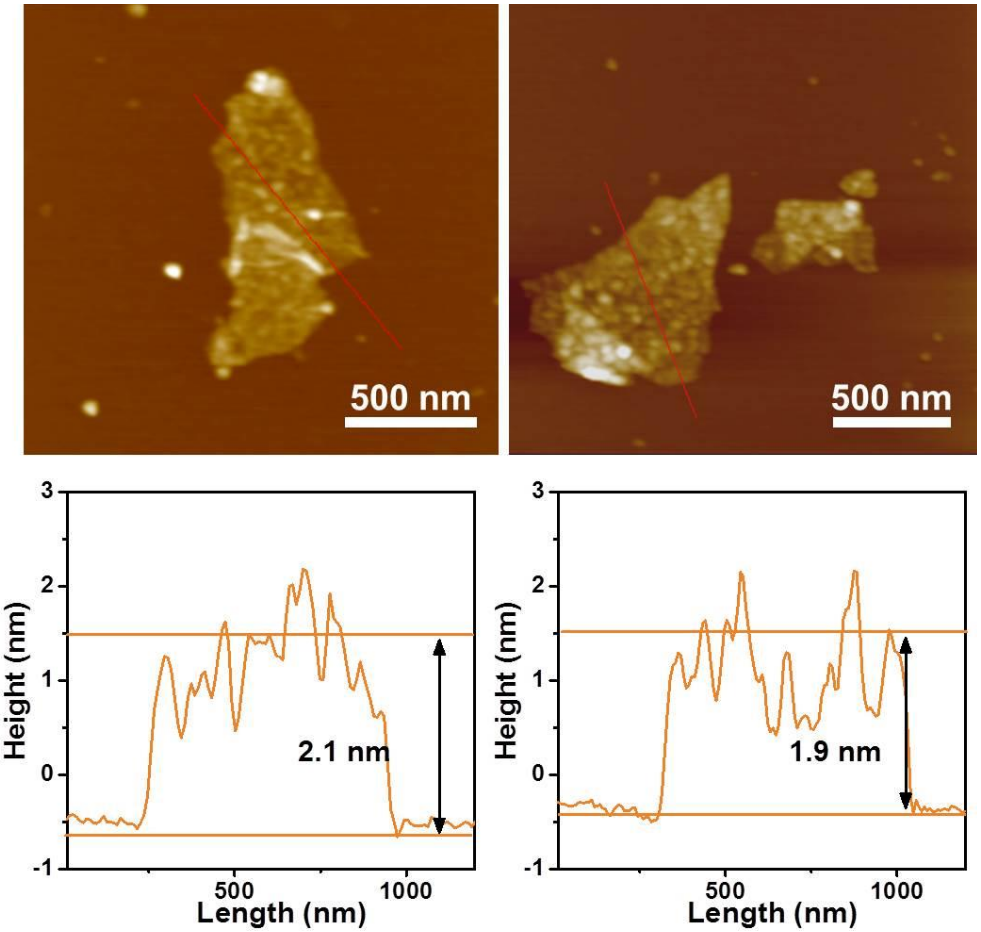

Fig. S14 Atomic force microscopy (AFM) images and height profiles of Ni-B_i/50%G.

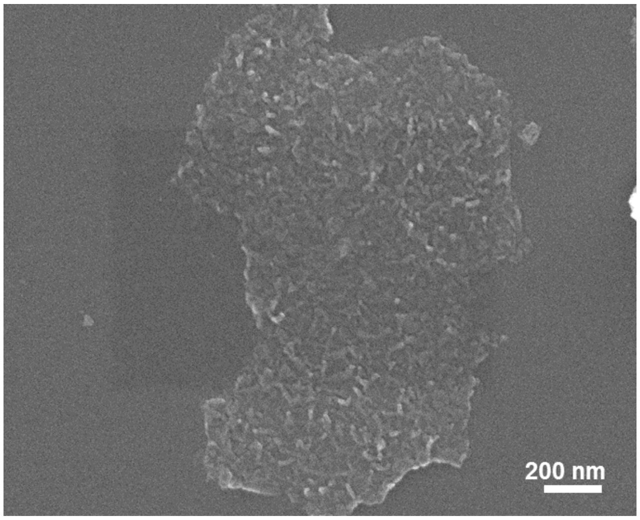

Fig. S15 Scanning electron microscopy (SEM) image of Ni-B$_i$/30%G after photocatalytic activity test.

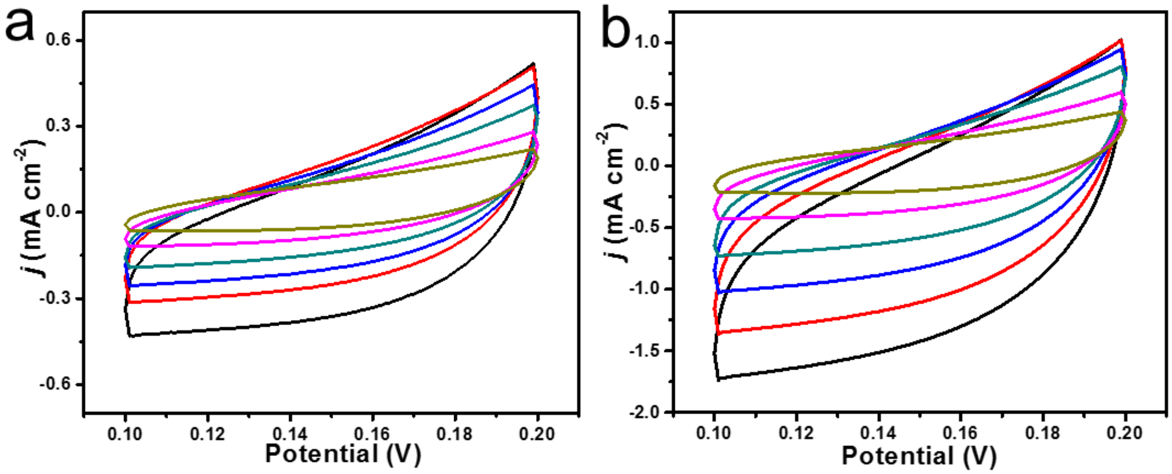

Fig. S16 Cyclic voltammetry (CV) curves measured at different scan rates from 10 to 100 mV s^{-1} in 1 M KOH for Ni-B$_i$ (a) and Ni-B$_i$/G heterostructure (b).

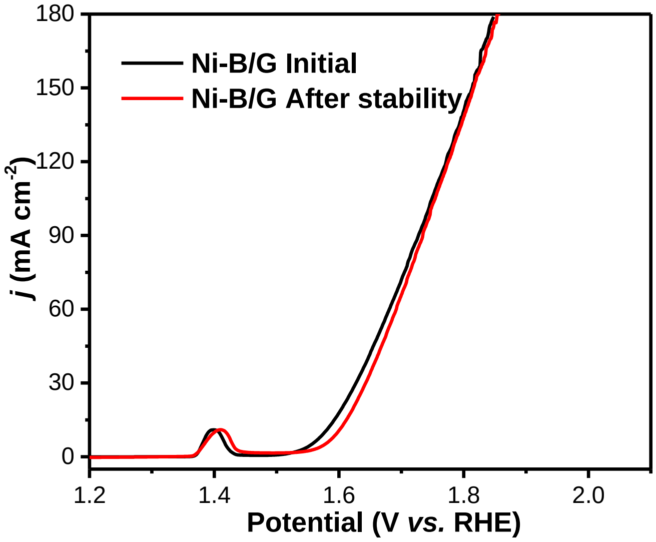

Fig. S17 Linear sweep voltammetry curves of Ni-B$_i$/G heterostructure before and after stability test.

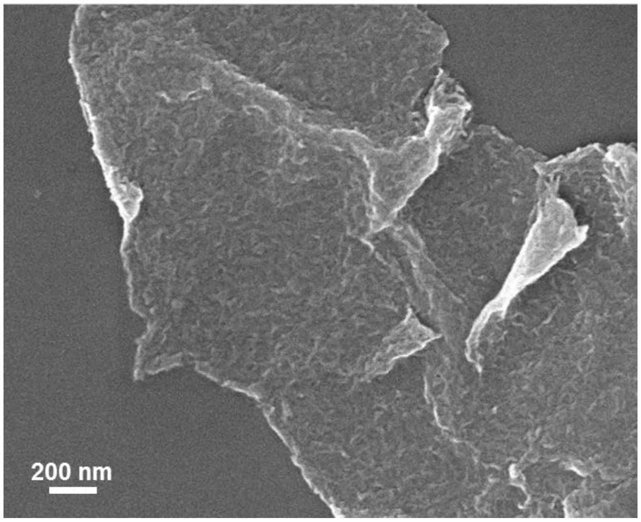

Fig. S18 Scanning electron microscopy (SEM) image of Ni-B$_i$/30%G after electrocatalytic activity test.

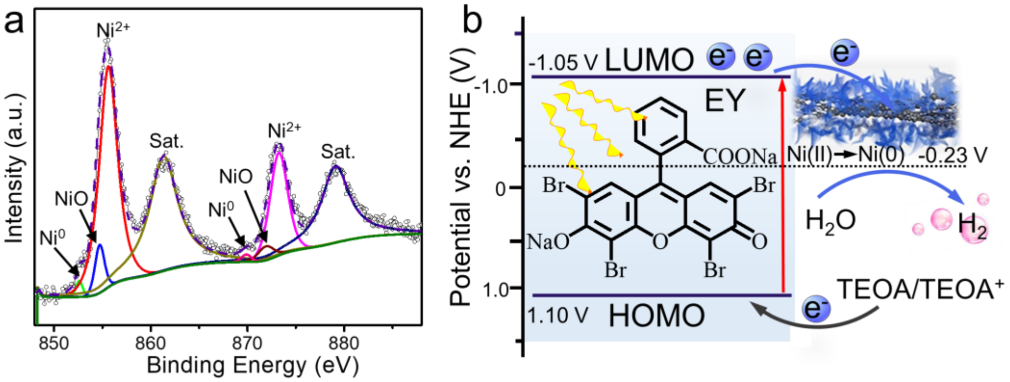

Fig. S19 (a) X-ray photoelectron (XPS) analysis of Ni 2p of Ni-B$_i$/G after photocatalytic activity test. (b) Schematic illustration on the photocatalytic hydrogen production over EY sensitized Ni-B$_i$/G system.

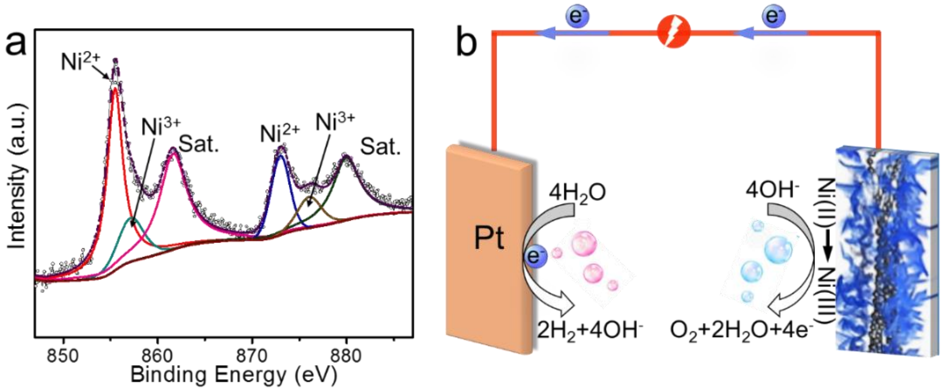

Fig. S20. (a) X-ray photoelectron (XPS) analysis of Ni 2p of Ni-B$_i$/G after electrocatalytic activity test. (b) Schematic illustration on the electrocatalytic oxygen evolution over Ni-B$_i$/G sandwich heterostructure.

References

S1. L. Liu and L. Hong, *Catal. Today*, 2016, **263**, 52-60.

S2. J. Ding, W. Yan, W. Xie, S. Sun, J. Bao and C. Gao, *Nanoscale*, 2014, **6**, 2299-2306.

S3. H. Wang, H. Yi, X. Chen and X. Wang, *J. Mater. Chem. A*, 2014, **2**, 1165-1173.

S4. M.-Q. Yang, C. Han, N. Zhang and Y.-J. Xu, *Nanoscale*, 2015, **7**, 18062-18070.